Alma Mater Studiorum Università di Bologna
Archivio istituzionale della ricerca

A Ka-Band MMIC LNA in GaN-on-Si 100-nm Technology for High Dynamic Range Radar Receivers

(Article begins on next page)

18 April 2024

Rights / License:

A Ka-Band MMIC LNA in GaN-on-Si 100-nm Technology for High Dynamic Range Radar Receivers

C. Florian, *Member, IEEE*, P. A. Traverso, *Member, IEEE* and A. Santarelli, *Member, IEEE*

Abstract— A Ka-band monolithic low noise amplifier (LNA) with high gain and high dynamic range has been designed and implemented in a 100-nm GaN-on-Si technology. The LNA is designed as the first stage of a high dynamic range receiver in a FMCW radar for the detection of small drones. The 3-stage MMIC LNA has a linear gain of 26 dB and a noise figure (NF) of 2 dB in the frequency band 33-38 GHz. Output P1dB and output IP3 at 37 GHz are 20 dBm and 28.4 dBm, respectively. To our knowledge this combination of NF, gain and dynamic range performance represent the state of art in this frequency band.

Index Terms— LNA, Low noise amplifier, Ka-band, GaN-on-Si, radar receiver, drone detection, high dynamic range.

I. INTRODUCTION

THE detection of UAVs of small dimensions has recently become a very important topic, due to the diffusion of low-cost drones that represent an increasing potential risk for security [1][2]. The FMCW radar is considered one of the most suitable solution for drone detection because of its architectural simplicity and short-range detection capability [1]-[4]. The detection of small drones represents a challenging task, since their very limited dimensions and non-reflective material composition imply very small radar cross sections (RCS). For this reason, the optimization of the radar detection range and resolution can be pursued only by exploiting millimeter wave frequencies, high transmitted power, and receivers with low noise figure (NF) and high dynamic range. In this context, Gallium Nitride (GaN) microwave technologies represent the best solution in terms of performance, since they offer state-of-the-art figure of merits for both the transmitter and receiver microwave front ends [4]-[6]. The exploitation of the superior GaN power density at microwave frequencies is an advantage for the implementation of compact, high-power transmitters needed to increase the weak echo signal of the drone target (low RCS). On the other hand, GaN technology is also very attractive in the RX section, due to the combination of both low noise and wide dynamic range characteristics [5]-[9]. This feature is of primary importance in a FMCW radar receiver for drone detection, since the LNA needs to detect very low drone-echo signals (close to the thermal noise level), while maintaining its linearity even in presence of strong interferer/blocking signals, which are typically due to radar clutter and the leakage of the power amplifier of its own transmitter [3][4]. In this paper, we describe a GaN-based, Ka-band MMIC LNA to be exploited in the receiver of a FMCW radar for small drone detection. The adoption of mmW-GaN technology enables to simultaneously target low NF, high gain, and large dynamic range, leading to unparalleled combined performance in upper Ka band.

II. LNA SPECIFICATIONS AND TECHNOLOGY

The LNA was designed in the framework of a research project aimed at the development of the microwave front end for a FMCW radar capable of detecting small drones with RCS as low as 1 cm^2 at the maximum range of 2 kilometres. To this goal, the selected operative frequency is 35-37 GHz with a transmitted power of 37 dBm [4]. System-level analyses of the radar [4] indicate that the LNA should have a NF below 2.5 dB and a linear gain exceeding 20 dB. Moreover, the LNA needs to operate in presence of a fixed strong interference at its input: due to the TX-RX isolation of the system that is limited to 52 dB [10], a blocking signal of -15 dBm (HPA leakage) is constantly applied to the LNA input, whereas the useful radar signal can be as low as -147 dBm. In addition to the PA leakage (strongest interferer) many other objects in the surrounding environment represent interferers for the LNA (e.g. buildings, vehicles, trees, birds): all these signals represent radar clutter that, mixing up with the drone signal, create intermodulation (IM) products that can have similar power level of the drone echo signal. To minimize these effects, high dynamic range of the LNA is highly desirable to minimize IM products that are potentially false targets. GaN millimetre wave MMIC technology is selected to simultaneously target high sensitivity and high dynamic range for the radar receiver. The commercial MMIC process selected for the LNA design is the D01GH GaN-on-Si process by OMMIC foundry [5]. The process features a 100-nm mushroom-gate HEMT with f_T=105 GHz. At 35 GHz and V_{DS} = 12 V, the typical power density is 3.3 W/mm, with a maximum stable gain of 13 dB (2×25μm device). The breakdown voltage is 50 V and the maximum drain current density is 1.3 A/mm. The minimum NF of a 2x30 μm HEMT with V_{DS} = 5V at 36 GHz is 1.25 dB with an associated gain of 10 dB. The technology includes high/low density MIM capacitors, spiral inductors, 3 level of metal interconnections, metal resistors, air bridges and via holes.

III. LNA DESIGN

The design was carried out exploiting the foundry design kit. The LNA topology is described in Fig. 1. It is a single-ended 3-stage amplifier with a single device for each stage. Large periphery devices are used to improve dynamic range, while maintaining a reasonably low NF. Devices' periphery and bias points were selected as a compromise between NF, gain, dynamic range, matching loss and stability. The selected devices are 6x30-μm, 8x40-μm and 8x50-μm HEMTs for the first, second and third stage, respectively. The devices are biased with a low current density of 105 mA/mm (about

$I_{DSS}/10$), for a corresponding V_G = -1.25 V at V_{DS} = 6 V. Bias currents are I_{D1} = 19 mA, I_{D2} = 33 mA, I_{D3} = 42 mA for a total power consumption: 564 mW. The dimensions of the source via holes, and thus their parasitic inductance, were optimized by means of EM simulations to make the optimum source impedances for noise and gain as close as possible. In Fig. 2, the optimum source impedances for noise (Z_S noise) and gain (Z_S gain) are shown in the design frequency band for each device. In the charts, the impedance synthesized by the respective matching network are shown with the blue lines. Finally, in the Smith charts of Fig. 2, also the associated load for maximum gain is listed (Z_L opt). "Z_S noise" and "Z_S gain" are quite close, so that matching for noise does not imply a severe loss of available gain. The design choice was to synthesize the optimum source impedance for noise for the first two stages, with the corresponding Z_L opt for gain maximization. For the last stage, the synthesized source impedance is a compromise between noise and gain optimization, whereas the selected load was not the one for maximum gain, but for distortion minimization (Z_L for IP3 in the figure). The simulated NF and gains obtained for each stage from this design strategy are listed in Fig. 1, along with the NFmin, associated gain (G_{ASS}) and maximum available gain (MAG) of the source-grounded devices.
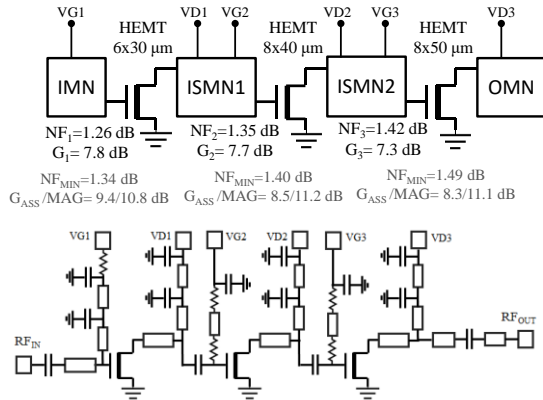

Fig. 1. Structure of the 3-stages Ka-band LNA, with NF and gain for the HEMT of every stage before and after source degeneration.

A special effort was carried out to minimize the matching losses, which are particularly important for the first stage for the direct deterioration of the LNA NF [11]. This task is a bit aggravated by the use of a silicon substrate, which is more lossy than SiC. Loss minimization was pursued by optimization of the matching and bias network topologies that are kept as simple as possible (trade off with matching bandwidth). The simulated loss for the input matching network is 0.2 dB. This was done sacrificing out-of-band response.
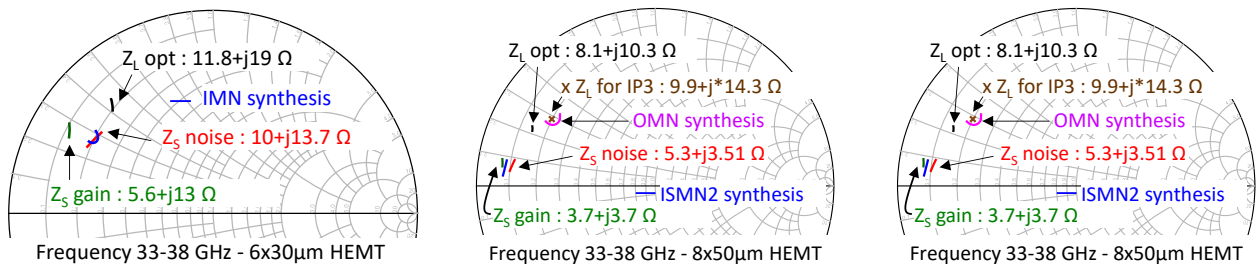
Large signal simulations were carried out for the evaluation of the LNA dynamic range. As an example, the large signal intrinsic load lines of the three devices are shown is Fig. 3. From these plots the clipping of the load lines at increasing input power (P_{IN}), which is one of the main sources of nonlinearity, can be evaluated. HEMT's peripheries for DR maximization were selected with this analysis. The thin (red) curves represent the load line evolution at increasing LNA input power (P_{IN}) up to 10 dBm, whereas the thick (black) curve is the load line corresponding to an input power P_{IN} = -2 dBm.

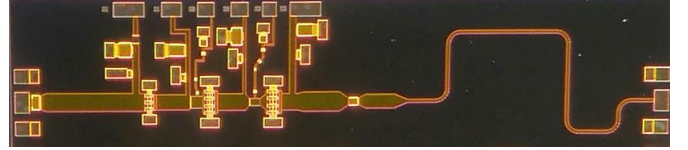## IV. IMPLEMENTATION AND MEASUREMENT

Fig. 4. Picture of the LNA: chip dimensions are 5 mm x 1.1 mm.

The picture of the MMIC is shown in Fig. 4. The chip dimension ratio is unusual, with an unnecessary large space occupied by the output matching network: this was done exclusively to match the horizontal dimension of other MMIC in the multi-project wafer tile. The test jig implemented for the LNA characterization is shown in Fig. 5.
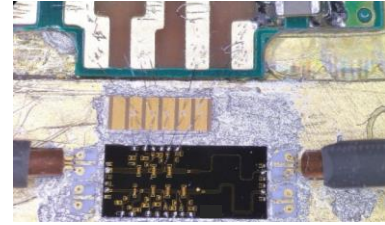

Fig. 5. Test jig under the probe station.

External GSG-microstrip adapter on alumina are adopted to include RF wire bonding in the measurement with GSG probes. Measured S parameter are shown in Fig. 6, along with simulations. The LNA features about 26 dB of gain and input and output matching better of -7 and -10 dB respectively, in the 33-38 GHz frequency band. Gain is about 6 dB higher than expected. From our analyses, this is mainly due to an overestimation of source degeneration effect ascribable to issues in via-holes EM simulations, and to some inaccuracy of the active device models with respect to process parameter dispersion. The chip exhibits gain also at Ku band: this could have been prevented by modification in matching networks, but we decided to avoid any added complexity to them to optimize in-band performance.
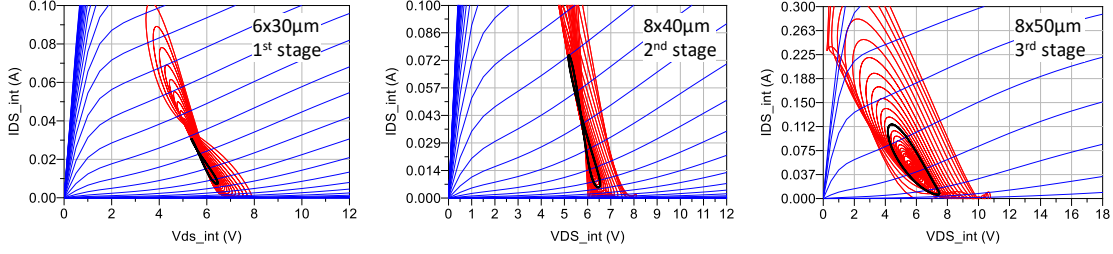

Fig. 2. Design matching impedances for the devices of the three stages in the design frequency band. Listed values are at 37 GHz.

Fig. 3. Simulations of HEMTs' intrinsic load lines at different P_{IN} (thin red lines). Thick black curves are the load lines corresponding to P_{IN} = - 2 dBm.

Nonetheless, this is not an issue, since it is filtered out by other narrowband components in the receiver chain. The measured noise figure of the LNA in shown in Fig. 7 with a comparison with simulations. In Fig. 8, the large signal characterization of the LNA is shown at 37 GHz. The input and output P1dB
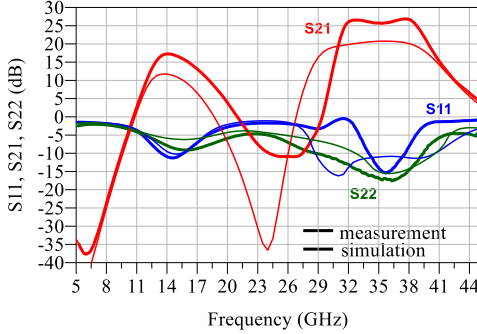

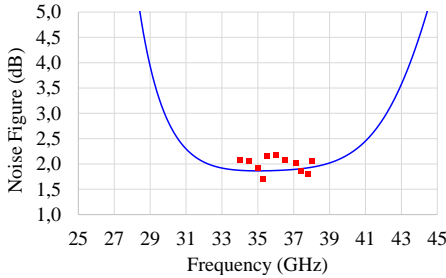Fig. 6. Measured S-parameters and comparison with simulations.

Fig. 7. Measured noise figure and comparison with simulations.

are -5 dBm (simulated 3.7 dB) and 20 dBm (sim. 22.8 dB), respectively. The measured input and output IP3 are 2.4 dBm (sim. 10 dBm) and 28.4 dBm (sim. 29 dBm), respectively. Due to the 6-dB gain difference, the comparison of LS performance with simulations proposed in Fig. 8 is accomplished by shifting by 6 dB the x-axis for simulation data. Input P1dB/IP3 are clearly lower than predicted due to the measured higher gain (see Fig. 6). Fig. 9 shows the result of two-tone intermodulation measurement. Table I lists comparable MMIC LNAs at Ka-band. Simulation-only publications are not included in the table; nonetheless the design described in [17] represents a confirmation of the capability of this process to simultaneously address low noise behaviour and high dynamic range. LNAs with small dynamic range (and very low power consumption) are not included in the table, since are not significant for this application. Those LNAs exploit InP/GaAs HEMT/mHEMT, SiGe or Si-CMOS processes and are typically applied in radioastronomy, satellite and, recently, 5G communications. To our knowledge, the combination of gain (25 dB), NF (2dB),

P1dB (20 dBm) and IP3 (28.4 dBm) of this circuit represents the state-of-the-art of measured results at Ka band.
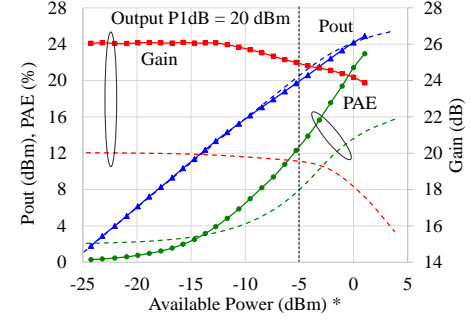

Fig. 8. Measured and simulated (dashed) LS behavior of the LNA at 37 GHz. * for simulated data x-axis is shifted by 6 dB to compare curves
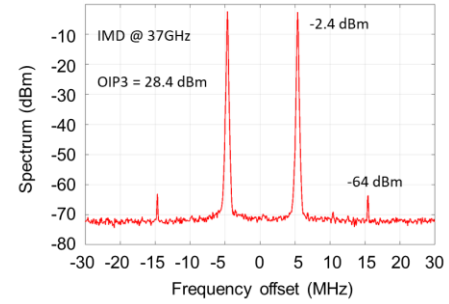

Fig. 9. Measured IMD at 37 GHz (10 MHz tone spacing).

TABLE I
STATE-OF-THE-ART FOR MMIC LNA @ KA BAND

Ref.	Tech.	BW (GHz)	Gain (dB)	NF (dB)	OP1dB (dBm)	OIP3 (dBm)
t. w.	GaN on Si	[33-38]	26	2.0	20	28.4
[12]	GaN on SiC	[27-29]	20	4.0	12.5	n.a.
[13]	GaN on SiC	[30-40]	25	1.5	11	20.5
[14]	CMOS SOI	[24-28]	12.8	1.6	n.a.	16.8
[15]	GaN on Si*	[22-30]	13	1.5	21	n.a.
[16]	GaN on Si	[18-31]	22	1.9	16	28
vendor	part #	BW (GHz)	Gain (dB)	NF (dB)	OP1dB (dBm)	OIP3 (dBm)
OMMIC	CGY2250U*	[26-34]	20	1.6	17	n.a.
UMS	CHA2391	[36-40]	15	2.5	12	20
AD	HMC566	[29-36]	21	2.8	13	24.5
QORVO	TGA4508	[30-42]	21	2.8	14	n.a.
QORVO	CMD162	[26-34]	22	1.7	7	14

t.w.: this work   -   * same process of this work

REFERENCES

[1] J. Drozdowicz et al., "35 GHz FMCW drone detection system," 2016 17th International Radar Symposium (IRS), Krakow, 2016, pp. 1-4.

[2] M. Caris, W. Johannes, S. Sieger, V. Port and S. Stanko, "Detection of small UAS with W-band radar," 2017 18th International Radar Symposium (IRS), Prague, 2017, pp. 1-6.

[3] Brooker, G. M., "Understanding millimetre wave FMCW radars," in 1st International Conference on Sensing Technology, Palmerston North, New Zealand, November, 2005.

[4] A. Cidronali et al., "System Level Analysis of Millimetre-wave GaN-based MIMO Radar for Detection of Micro Unmanned Aerial Vehicles," 2019 PhotonIcs & Electromagnetics Research Symposium - Spring (PIERS-Spring), Rome, Italy, 2019, pp. 438-450.

[5] R. Leblanc et al., "6W Ka Band Power Amplifier and 1.2dB NF X-Band Amplifier Using a 100nm GaN/Si Process," 2016 IEEE Compound Semiconductor Integrated Circuit Symposium (CSICS), Austin, TX, 2016, pp. 1-4.

[6] E. Limiti et al., "T/R modules front-end integration in GaN technology," 2015 IEEE 16th Annual Wireless and Microwave Technology Conference (WAMICON), Cocoa Beach, FL, 2015, pp. 1-6.

[7] Marc van Heijningen et al. "C-Band Single-Chip Radar Front-End in AlGaN/GaN Technology", Microwave Theory and Techniques IEEE Transactions on, vol. 65, no. 11, pp. 4428-4437, 2017.

[8] S. Masuda et al., "GaN single-chip transceiver frontend MMIC for X-band applications," 2012 IEEE/MTT-S International Microwave Symposium Digest, Montreal, QC, 2012, pp. 1-3.

[9] P. Schuh, H. Sledzik and R. Reber, "High performance GaN single-chip frontend for compact X-band AESA systems," 2017 12th European Microwave Integrated Circuits Conference (EuMIC), Nuremberg, 2017, pp. 41-44.

[10] M. Wahab, Y. P. Saputera, Y. Wahyu and A. Munir, "Isolation improvement for x-band FMCW radar transmit and receive antennas," 2016 International Conference on Radar, Antenna, Microwave, Electronics, and Telecommunications (ICRAMET), Jakarta, 2016, pp. 110-114.

[11] D. Resca et al., "A robust Ku-band low noise amplifier using an industrial 0.25-?m AlGaN/GaN on SiC process," (2013) European Microwave Week 2013, EuMW 2013, art. no. 6687894, pp. 496-499.

[12] E. M. Suijker et al., "Robust AlGaN/GaN Low Noise Amplifier MMICs for C-, Ku- and Ka-Band Space Applications," 2009 Annual IEEE Compound Semiconductor Integrated Circuit Symposium, Greensboro, NC, 2009, pp. 1-4.

[13] M. Micovic et al., "Ka-Band LNA MMIC's Realized in Fmax > 580 GHz GaN HEMT Technology," 2016 IEEE Compound Semiconductor Integrated Circuit Symposium (CSICS), Austin, TX, 2016, pp. 1-4.

[14] C. Li, O. El-Aassar, A. Kumar, M. Boenke and G. M. Rebeiz, "LNA Design with CMOS SOI Process-l.4dB NF K/Ka band LNA," 2018 IEEE/MTT-S International Microwave Symposium - IMS, Philadelphia, PA, 2018, pp. 1484-1486.

[15] X. Tong, R. Wang, S. Zhang, J. Xu, P. Zheng and F. Chen, "Degradation of Ka-Band GaN LNA Under High-Input Power Stress: Experimental and Theoretical Insights," in IEEE Transactions on Electron Devices, vol. 66, no. 12, pp. 5091-5096, Dec. 2019.

[16] X. Tong, S. Zhang, P. Zheng, J. Xu and X. Shi, "18–31 GHz GaN MMIC LNA using a 0.1 um T-gate HEMT process," 2018 22nd International Microwave and Radar Conference (MIKON), Poznan, 2018, pp. 500-503.

[17] L. Pace, W. Ciccognani, S. Colangeli, P. E. Longhi, E. Limiti and R. Leblanc, "A Ka-Band Low-Noise Amplifier for Space Applications in a 100 nm GaN on Si technology," 2019 15th Conference on Ph.D Research in Microelectronics and Electronics (PRIME), Lausanne, Switzerland, 2019, pp. 161-164.